Polymer 281 (2023) 126113

Contents lists available at ScienceDirect

Polymer

journal homepage: www.elsevier.com/locate/polymer

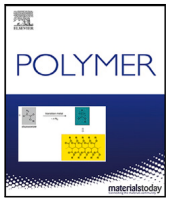

Filler-induced heterogeneous nucleation of polymer crystals investigated by molecular dynamics simulations

Dominic Wadkin-Snaith *, Paul Mulheran, Karen Johnston

Department of Chemical and Process Engineering, University of Strathclyde, Glasgow G1 1XJ, United Kingdom

ARTICLE INFO

Keywords:
Polymer physics
Semi-crystalline polymers
Molecular dynamics simulations

ABSTRACT

Filler particles are known to act as nucleants for polymer crystallisation yet the connection between the filler surface properties and polymer crystallisation are not well understood. In this work, molecular dynamics simulations were used to investigate homogeneous and heterogeneous polymer nucleation and crystallisation using a generic linear bead–spring polymer model with a bond bending potential. The polymer systems were equilibrated at high temperature and then cooled at a constant rate. Without a surface present, polymers with stiff chains were found to crystallise more readily than more flexible polymers. The degree of crystallinity was estimated based on the mass fraction of straight chain segments which we equate to stem mass fraction. At a temperature T_c a sharp increase in density, radius of gyration and stem mass fraction occurred. After cooling, the systems were reheated and some systems showed hysteresis with a sharp decrease in these properties occurring upon melting at $T_m > T_c$. For slower heating rates, crystal growth occurred during heating from between the glass transition temperature, T_g, and T_c until just before melting at T_m. The presence of an isotropic surface was found to promote crystallisation in flexible systems that did not crystallise in the bulk, where the stem mass fraction and T_c increased with the interaction strength between the surface and the polymer beads. Changes in T_c and degree of crystallinity with cooling rate are consistent with experimental observations. This model captures polymer crystallisation phenomena and provides insight into heterogeneous nucleation, demonstrating that strong interfacial interactions promote crystallisation, thus aiding the choice or design of nucleants for control of polymer crystallisation and microstructure.

1. Introduction

Plastics are used in a wide range of applications including aerospace, electronics, healthcare technologies and packaging. Plastics are often made of thermoplastic polymers that are semi-crystalline, and the crystallinity and microstructure of the polymer influences key properties of the polymer such as mechanical strength and gas/water vapour barrier. The properties of polymers are well known to be modified by adding filler particles. A study of fillers in polyhydroxybutyrate showed that filler surfaces act as nucleants but there were no clear trends on how particular filler materials or surfaces influence crystallisation [1]. In order to tailor polymer properties by selecting appropriate fillers, it is necessary to understand the polymer-filler interface and how it influences polymer properties such as crystallinity. Computer simulations can be used to provide insight into the interfacial properties, including polymer crystallisation and growth. A variety of computational approaches have been used to study polymer crystal nucleation and growth in the presence of surfaces [2–8]. Many of these studies have used molecular dynamics simulations with coarse grained (CG) models, such as united atom (UA) models [9] or bead spring models such as the Kremer–Grest (KG) model [10,11].

A UA model for alkanes was parameterised to study isothermal polymer crystallisation and growth by Waheed, et al. [2,3] on a corrugated surface. A melt system of C20 chains between two surfaces was quenched to below the melting temperature, and it was observed that the chains extended and formed an hexagonal packed structure, starting from the surfaces and growing towards the centre of the cell until the systems were fully crystalline. This study was extended to longer chains of length C50 and C100 [3]. In all cases, nucleation occurred at the surface, however, for the C100 system crystal growth proceeded more slowly and chains did not fully extend, with defects persisting in all layers until the end of the simulation.

Yamamoto [4] used a bead spring model to represent polymethylene for which every bead represented a united atom and each spring modelled by an harmonic potential to study isothermal crystallisation from even longer chain systems of C100 and C1000 between two corrugated surfaces. The C100 system was quenched to below the melting

* Corresponding author.
E-mail address: dominic.wadkin-snaith@strath.ac.uk (D. Wadkin-Snaith).

https://doi.org/10.1016/j.polymer.2023.126113
Received 7 March 2023; Received in revised form 19 May 2023; Accepted 12 June 2023
Available online 14 June 2023

temperature, and, as in the work of Waheed et al., nucleation occurred at the surface. However, in these simulations, tapered lamellae were observed growing towards the centre of the system, which could be due to the larger system size of 640 chains compared to 40 chain system of Waheed et al.. The lamella showed thickening growth along the chain axis as well as perpendicular growth. It was found that the rate of crystallisation increased with decreasing temperature until it reached a maximum, where at lower temperatures the chain mobility was restricted. Similar results were observed for the C1000 system.

A CG model for PVA [12,13] investigated crystallisation under isothermal and constant cooling conditions in bulk polymer systems. For a cooling and heating cycle, hysteresis was observed in the volume per monomer. Increasing chain stiffness acted as a driving force for lamella formation in the bulk polymer. This model was later used to study the effect surfaces on polymer crystallisation [8] for chains exceeding the entanglement weight. It was found that heterogenous nucleation occurred first, followed by then homogeneous nucleation. Two stages of homogeneous nucleation were observed, first nucleation occurred near the walls, then far from the walls, which was attributed to the longer entanglement lengths in the boundary regions. A similar effect is seen in a Monte Carlo study of a confined entangled thin film [14]. In this study nucleation occurred faster for attractive surfaces than for repulsive surfaces up to a critical interaction strength, beyond which crystal growth slowed down.

The KG model has been used to study the glass transition in ultra thin films at a smooth wall [5,6] where it was found that the melt did not crystallise, which was thought to be due to a mismatch between the bonded and non-bonded length scales. A study by Mackura and Simmons [7] did observe polymer heterogeneous nucleation using the KG model in the presence of an fcc lattice of Lennard-Jones beads, demonstrating that the KG model can be used to study heterogenous nucleation in the presence of a structured surface. These studies indicate that a KG model of unentangled polymer chains resist nucleation and growth in the bulk and also in the presence of smooth surfaces but does nucleate and crystallise in the presence of a structured surface.

In this work, we use a modified KG model to study the effect of chain stiffness and surface interaction strength on polymer crystallisation and nucleation. We first investigate how chain stiffness influences crystal nucleation in the bulk, and explore how the crystallinity is affected by cooling and heating cycles. We then choose a chain stiffness that does not readily crystallise in bulk and study the effect of surface interaction strength on heterogeneous nucleation. Although previous studies have investigated how surface-polymer interaction strength affects crystallisation, these have generally been limited to very thin films where confinement also plays a role. In this study, the bulk polymer melt is between two filler surfaces whose separation greatly exceeds the dimension of the polymer chains to avoid confinement effects. In addition we present heating and cooling cycles in the presence of filler surfaces, which has studied previously only for a bulk polymer system. Finally, we discuss the free energy of the system, and compare our results with experimentally observed phenomenon.

2. Methodology

2.1. Polymer and surface models

We use classical molecular dynamics (MD) simulations to simulate polymer crystallisation at a surface. The polymer is represented by a modified Kremer–Grest (KG) model [10] where parameters and degrees of freedom are in Lennard-Jones units. In the KG model, bond stretches are modelled by the finite-elastic-non-extensible spring (FENE) potential

$$U_{\text{bond}}(r) = -\frac{1}{2}\kappa_{\text{r}} r_0^2 \ln\left[1 - \left(\frac{r}{r_0}\right)^2\right] \tag{1}$$

where r is the distance between bonded atoms, and $\kappa_{\text{r}} = 30$ and $r_0 = 1.5$ are the FENE parameters.

We have modified the KG model by including an angle bending potential defined as

$$U_{\text{bend}}(\theta) = \kappa_\theta\left(1 - \cos\left(\theta - \theta_0\right)\right) \tag{2}$$

where θ is the bond angle and κ_θ is the angle potential strength, corresponding to chain stiffness. The constant κ_θ contains the usual factor of $\frac{1}{2}$ as implemented in LAMMPS. Here $\theta_0 = 180^{\text{o}}$ is the equilibrium angle in degrees, chosen to favour straight chain segments required for nucleation.

In the original KG model, non-bonded interactions are represented by the Weeks–Chandler–Andersen potential, which is a purely repulsive interaction between all beads. However, a purely repulsive non-bonded interaction can lead to a negative coefficient of expansion [15] and thus we have used a Lennard-Jones (LJ) potential which is shifted to be zero at the cutoff distance of $r_c = 2.5$. The LJ potential parameters are $\epsilon = 1$ and $\sigma = 1$.

$$\begin{aligned} U_{\text{non-bond}}(r) &= 4\epsilon\left[\left(\frac{\sigma}{r}\right)^{12} - \left(\frac{\sigma}{r}\right)^{6}\right] + C && r < r_{\text{c}} \\ &= 0 && r > r_{\text{c}} \end{aligned} \tag{3}$$

where C is chosen such that the potential is zero at the cut off distance, r_{c}.

The filler surface is represented by an LJ 9–3 smooth wall potential of the form

$$E_{\text{wall}}(z) = \epsilon_{\text{w}}\left[\frac{2}{15}\left(\frac{\sigma_{\text{w}}}{z}\right)^9 - \left(\frac{\sigma_{\text{w}}}{z}\right)^3\right] \tag{4}$$

where z is the perpendicular distance of the polymer bead from the wall, the wall potential is cutoff distance is $r_c = 2.5$. We set $\sigma_{\text{w}} = 1$, and ϵ_{w} was varied to control the strength of the wall-bead interaction. The smooth walls are placed at the top and bottom of the simulation cell.

2.2. System setup and simulation details

MD simulations were performed using the LAMMPS package [16]. To setup the initial simulation a 20-bead chain is first relaxed in a vacuum. The coiled chain is then inserted into a cuboidal simulation box of size $52.040 \times 27.903 \times 20.155\ \sigma^3$ with a random position and orientation. This process is repeated until the simulation box contains 800 chains. Periodic boundary conditions were applied in the x, y and z directions. For the simulations with filler particle surfaces, walls are placed at the top and bottom of the simulation box (in the x–y plane) with periodic boundary conditions applied in the x and y directions.

To remove high energy conformations the system is relaxed using a short NVT simulation at $T^* = 1.2$ for 1×10^4 timesteps, corresponding to $10^2\ \tau$, where

$$\tau = \sqrt{\frac{m\sigma^2}{\epsilon}}.$$

is the LJ unit of time, with $m = 1$ being the mass of a bead. We use a reduced dimensionless T^*, which is defined as $k_{\text{B}}T/\epsilon$, and from here onwards we simply refer to the reduced temperature as T. The NVT simulation is followed by an NPT simulation at $T = 1.2$ for a duration of 1×10^7 timesteps ($10^5\tau$), which is sufficient for the density and radius of gyration to reach a steady state. For both the NVT and NPT simulations the temperature is controlled by the Nose–Hoover thermostat with a damping time set to $2\ \tau$. For the NPT simulations the pressure is controlled by the Nose–Hoover barostat at $P = 0$ with a damping time of $2\ \tau$. For the NPT simulations, the simulation box is fixed in the y and z dimensions and allowed to vary in the x dimension. To nucleate crystal structures and obtain a crystal temperature, T_{c}, the equilibrated system was cooled from $T = 1.2$ to $T = 0.35$ at a cooling rate of $\Gamma_0 = 10^{-6}\ T\ \tau^{-1}$ in the NPT ensemble.

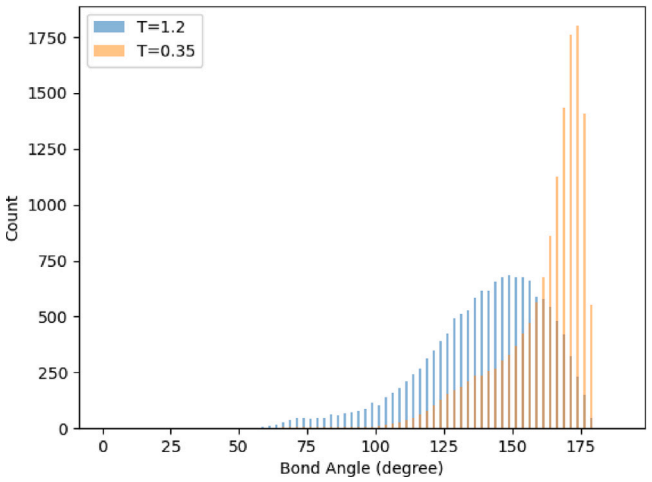

Fig. 1. Angle distributions for the $\kappa_\theta = 4$ melt for the start ($T = 1.2$) and end ($T = 0.35$) of the cooling run.

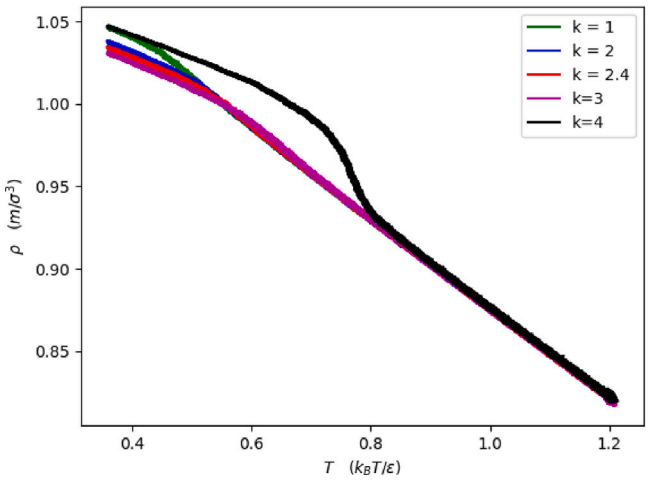

Fig. 2. Density as a function of temperature during cooling for different κ_θ values.

2.3. Analysis

Simulations were visualised using VMD [17]. To detect structural changes that could indicate glass transition or crystallisation the density and radius of gyration were measured with time. In the literature [18], authors often use the order parameter P2 as a function of bond vector to detect the onset of local order. Here we will take a different approach to detecting ordered regions, but note that similar results should be obtained for any appropriate method. For a quantitative analysis of crystal fraction, the number of beads belonging to straight segments of chains were counted. This approach measures every bond angle, θ, for every polymer in the simulation and labels the central bead defining a given bond angle as "straight" if the angle is greater than $\theta_{\text{cut}} = 162°$. The value of θ_{cut} was selected based on the angle distribution in the simulation with $\kappa_\theta = 4$ as this system crystallises upon cooling and, therefore, gives a guide to the angle distribution in both the melt and crystalline systems. The angle distributions are shown in Fig. 1 for $T = 1.2$ when the system is amorphous, and $T = 0.35$ when the system is partially crystalline. The selection of $\theta_{\text{cut}} = 162°$ corresponds to the cross-over in distributions. For a further discussion of the selection of the cut-off angle, see supplementary information (SI) and Fig. 1 in SI, where we compare the effect of cut-off angle on stem mass fraction. We then defined the minimum number of bonds of a 'straight segment', which we will label as a 'stem', to be five, and the four beads in the middle of these were counted as belonging to the stem. See Fig. 2 in SI along with accompanying text for a discussion on why the minimum number of beads has been selected to be 4. The fraction of beads belonging to stems is then used to calculate the stem mass fraction, which is an indication of the degree of crystallinity of the system. Varying θ_{cut} by ±3° changes the measured stem mass fraction but does not change the temperature at which maximum growth is observed. Similarly, increasing the number of beads defining a "straight segment" above four leads to a decrease in total stem mass fraction, as expected, but does not alter the temperature at which the maximum stem growth rate occurs.

3. Results

In this section we first explore the effect of the bending potential on the crystallisation of the bulk melt. Once we identify a suitable value for κ_θ that does not readily lead to crystallisation in the bulk, we then use this model system to explore crystallisation at a surface. We explore the effect of cooling rate, chain stiffness, and wall interaction strength on crystal nucleation and growth.

3.1. Effect of chain stiffness on crystallisation of a bulk polymer melt

In this section we present the properties of polymer melts with different chain stiffness. Melts of varying chain stiffness were cooled from $T = 1.2$ to $T = 0.35$ at a rate of $\Gamma_0 = 10^{-6}\ T\ \tau^{-1}$. The density variation with temperature is shown in Fig. 2 and the density increases as the system is cooled. The glass transition is characterised by a decrease in the gradient of the density, which occurs around $T = 0.5$ for systems with $\kappa_\theta \leq 3$. In these systems, the glass transition temperature, T_g, increases with chain stiffness, which is consistent with a previous study by Shavit and Riggleman [19], although we note that an accurate evaluation of T_g would require a more thorough statistical analysis [20]. The behaviour of the $\kappa_\theta = 4$ system clearly deviates from the more flexible chain systems by acquiring a pronounced shoulder at a temperature far higher than the T_g of the other melts.

To understand this behaviour further, we show the variation of the average chain radius of gyration R_g with temperature in Fig. 3. At $T = 1.2$, melts with stiffer chains (higher κ_θ value) exhibit a larger R_g, which is to be expected due to the increased Kuhn (or persistence) length. The value of R_g then increases as the system is cooled until the temperature approaches and drops below T_g, where a plateau is observed and R_g remains approximately constant. For the stiffest chain, $\kappa_\theta = 4$, there is a large step in R_g at around $T = 0.8$, which we note occurs at the same temperature as the shoulder in the density observed in Fig. 2.

Next we present the stem mass fraction versus temperature in Fig. 4. For $\kappa_\theta = 1, 2$ and 2.4 a small stem mass fraction of around 0.02 or less is measured at the lowest temperature. For $\kappa_\theta = 3$ we see an increase in stem mass fraction to 0.04 at $T = 0.35$. This slight increase in stem mass fraction does not coincide with the glass transition observed for ρ or R_g. For the melt with $\kappa_\theta = 4$, there is a pronounced increase in stem mass fraction, which reaches around 0.38 at $T = 0.35$. This increase does coincide with the shoulders in density and R_g for this system at around $T = 0.8$.

These observations indicate clear differences in the behaviour of the different systems and this is most clearly seen from snapshots of the systems just after cooling. Fig. 5 shows images for the $\kappa_\theta = 2.4$ and $\kappa_\theta = 4$ melts, at $T = 0.35$. In the $\kappa_\theta = 4$ system, which has a stem mass fraction of 0.38, ordered regions are clearly visible. Together with the observed increase in density and R_g, it is clear that this system undergoes homogeneous crystallisation during cooling. For the $\kappa_\theta = 2.4$ melt, which has a small stem mass fraction of around 0.015 at $T = 0.35$, we can see that the stems are distributed randomly throughout the system and not ordered, and therefore, the stem mass fraction is not an indication of crystallisation in this case. This is also the case for the bulk systems with $\kappa_\theta < 2.4$. We conclude that for the $\kappa_\theta = 2.4$ bulk system crystallisation is not observed during cooling.

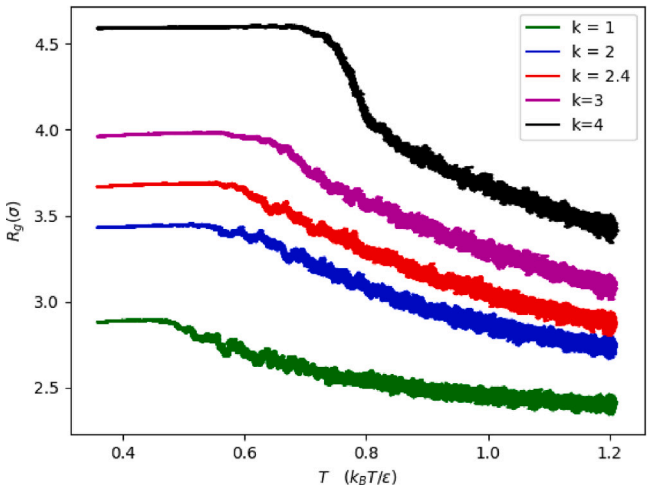

Fig. 3. Average radius of gyration as a function of temperature during cooling for different κ_θ values.

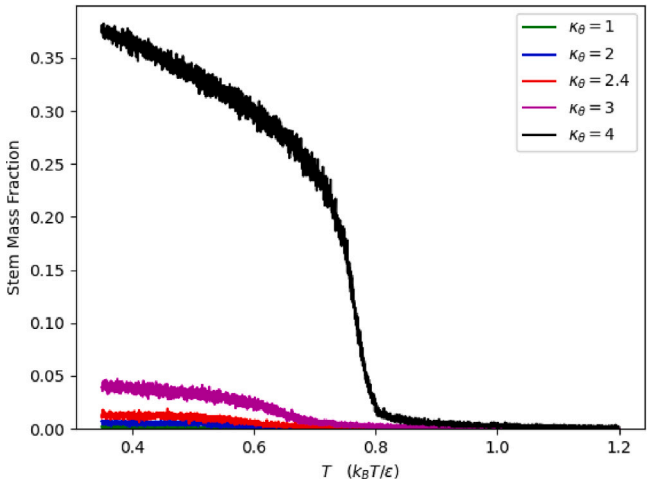

Fig. 4. Bead stem fraction as a function of temperature during cooling for different κ_θ values.

3.2. Cooling and heating cycle

We now explore the effect of heating the bulk melt systems after cooling. Fig. 6 shows the density, R_g and stem mass fraction versus temperature for a bulk melt with $\kappa_\theta = 2.4$ as the system is cooled from $T = 1.2$ down to $T = 0.35$ and then heated back up to $T = 1.2$ at the Γ_0 rate. The density curve on heating follows the density on cooling and $T_g \approx 0.54$. The R_g heating curve also follows closely the cooling curve, except for the region between T_g and $T_g + 0.1$ where R_g remains marginally higher in value, indicating the chains remain slightly extended before resuming the chain dimensions observed under cooling.

During cooling, the stem mass fraction remains close to zero for temperatures between 1.2 and 0.7. At $T \approx 0.7$ we observe a gradual increase in stem mass fraction until it arrests at around the glass transition temperature. A very slow growth in stem mass fraction is observed below the glass transition, which is attributed to local rearrangements. At $T = 0.35$ the stem mass fraction is just above 0.01, which corresponds to randomly distributed stem segments as discussed above. During heating the stem mass fraction follows the cooling curve, with a rapid decrease above T_g, which slows as the temperature increases.

Next we perform the same cooling and heating protocol on a bulk melt with $\kappa_\theta = 4$, shown in Fig. 7. As for the $\kappa_\theta = 2.4$ system, initially there is very little change in stem mass fraction on cooling until $T \approx 0.8$, when the stem mass fraction sharply increases to around 0.25 before resuming a gradual increase at $T \approx 0.7$, and reaches about 0.38 at $T = 0.35$, which exhibits ordered crystalline regions as presented previously in Fig. 5(b).

On heating from $T = 0.35$, all three physical quantities initially retrace the respective cooling curves until above $T \approx 0.7$ where the cooling and heating curves begin to deviate. For instance, the density only slowly decreases until $T \approx 1.05$, when it undergoes a sharp decrease that corresponds to crystal melting. Interestingly, R_g and the stem mass fraction both increase between $T = 0.74$ and $T = 0.86$. Between $T = 0.86$ and $T = 0.95$ a gradual decrease in stem mass fraction is accompanied by a slow down in the rate of increase of R_g. Between $T = 0.95$ and $T = 0.97$ growth in stem mass fraction proceeds before giving way to decline and then melting.

This crystal growth during heating, which is facilitated by an increase in mobility of chain segments before melting occurs, is observed experimentally as cold crystallisation. Hysteresis effects in polymer crystallisation during cooling and heating at constant rate have been previously observed for a coarse-grained PVA model [13] and a slight increase in long range ordering was also observed for one system just before melting occurred. Hysteresis is also seen in plots of specific volume for weakly entangled polymer melt simulations in [21], although we note that surfaces were not present in this study.

It is clear that crystallinity in the system leads to a strong hysteresis where the melting and crystallisation temperatures do not coincide. We note that we do not observe hysteresis for the $\kappa_\theta = 2.4$ melt in Fig. 6. We conclude that the $\kappa_\theta = 2.4$ system does not readily crystallise during cooling, which make this system a suitable choice to study the affect of a filler surface on crystal nucleation.

3.3. Effect of a surface on crystallisation

We now study the effect of a filler surface, using the smooth wall potentials at the top and bottom of the simulation cell. The wall interaction strength was initially chosen to be $\epsilon = 1.8$. As before, the system was equilibrated at $T = 1.2$, then cooled from 1.2 to 0.35 at a cooling rate of Γ_0, and then heated back up to 1.2 at a heating rate of Γ_0. Fig. 8 shows ρ, R_g and stem mass fraction versus temperature for cooling and heating.

During cooling, the density, radius of gyration, and stem mass fraction all exhibit a marked increase at $T \approx 0.66$ marked with a blue vertical line in Fig. 8, which corresponds to the crystallisation temperature T_c. At approximately $T = 0.55$ the density shows an inflection corresponding to T_g. When the system is cooled to $T = 0.35$ the stem mass fraction reaches its maximum value of around 0.12. On heating the system, the curves initially retrace the cooling curves, but above T_g the heating curves start to deviate from the cooling curve. The stem mass fraction undergoes a significant increase starting between T_g and T_c until around 0.75, when it starts to decline before the melting onset at approximately $T = 0.78$. R_g also slightly increases until around 0.75, as the chains become further extended during crystal growth. Similarly to the $\kappa_\theta = 4$ bulk system, the observed hysteresis appears to be a signature of crystallisation.

The simulation snapshots in Fig. 9 show the stems in the systems, providing further insight into this hysteresis effect. Fig. 9a) shows the stems during cooling at $T = 0.7$, and they are mostly randomly ordered in the centre of the simulation cell except for a few chains that are aligned with the surface. At $T = 0.35$, crystalline regions are seen at the surfaces in Fig. 9b), demonstrating that the surface has induced nucleation. During subsequent heating back up to $T = 0.7$ we can see in Fig. 9c) that the crystalline areas have further grown, facilitated by the increase in chain mobility above T_g.

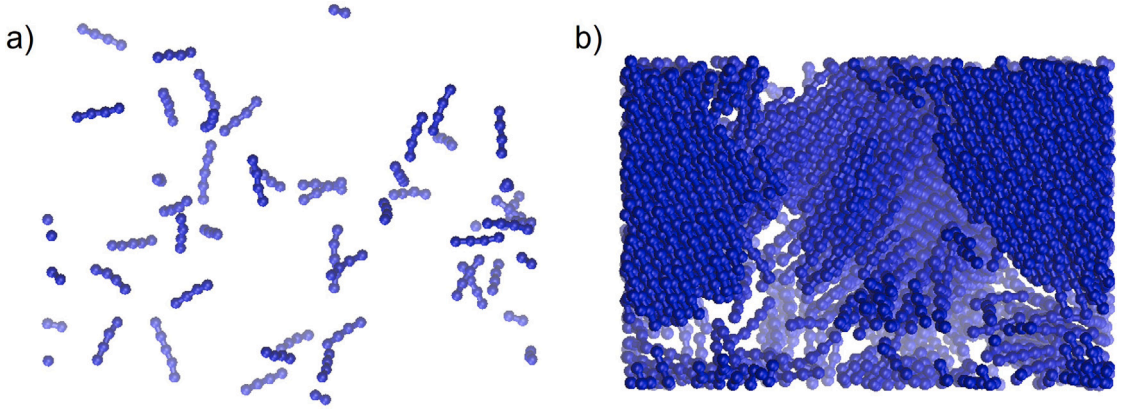

Fig. 5. Simulation snapshots only showing stems in the (a) $\kappa_\theta = 2.4$ and (b) $\kappa_\theta = 4$ bulk systems at $T = 0.35$, respectively. The absence of order of stems is clear in the $\kappa_\theta = 2.4$ system.

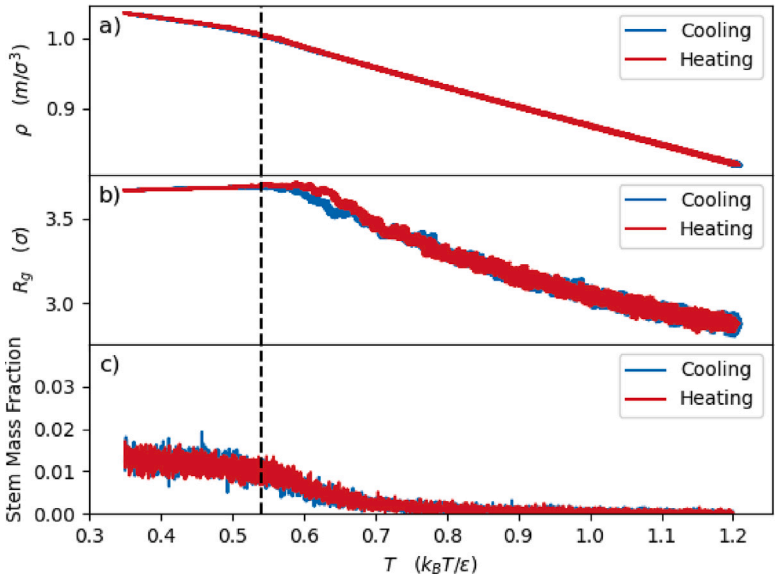

Fig. 6. Cooling and heating cycle for the $\kappa_\theta = 2.4$ system. The vertical line indicates the approximate glass transition temperature T_g.

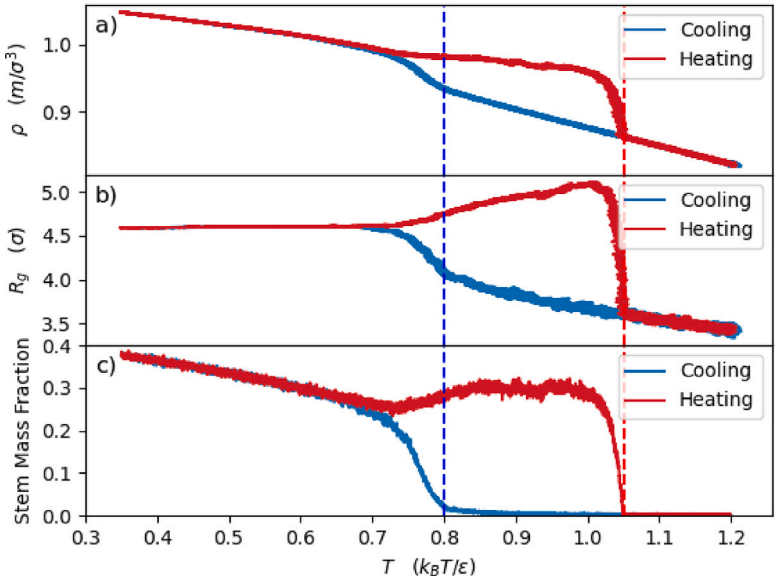

Fig. 7. Cooling and heating cycle for the $\kappa_\theta = 4$ system. The blue and red vertical lines indicate crystallisation and melting temperatures, respectively. (For interpretation of the references to colour in this figure legend, the reader is referred to the web version of this article.)

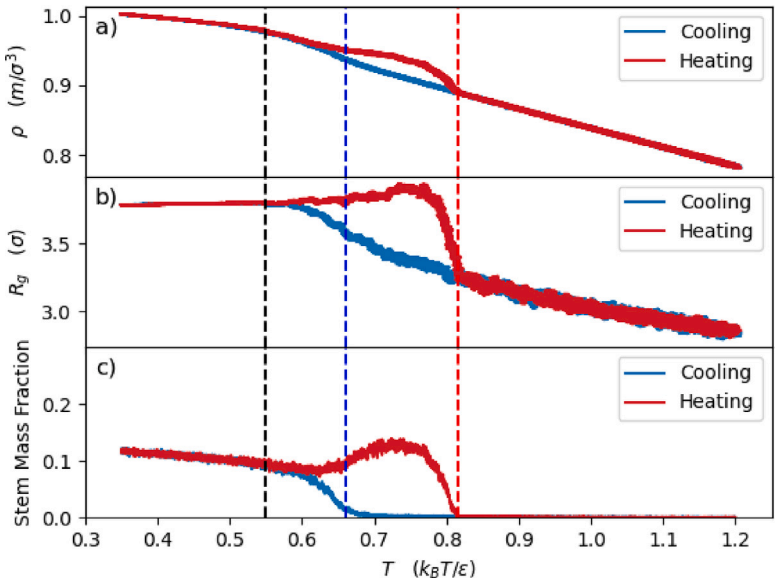

Fig. 8. Density ρ, radius of gyration R_g, and stem mass fraction vs temperature for the $\kappa_\theta = 2.4$ system between two walls. The black, blue and red lines indicate the approximate T_g, T_c and T_m, respectively. (For interpretation of the references to colour in this figure legend, the reader is referred to the web version of this article.)

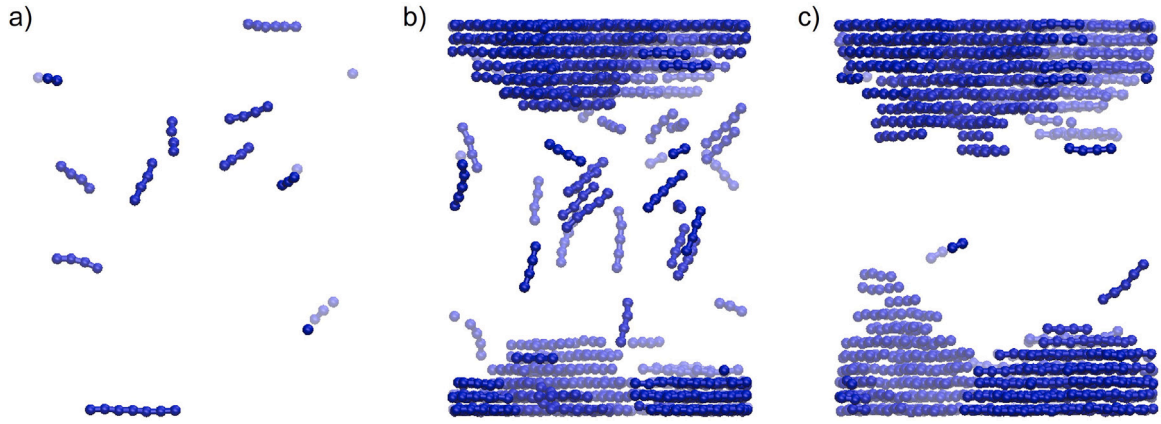

Fig. 9. The stems of the $\kappa_\theta = 2.4$ system at (a) $T = 0.7$ during cooling, (b) $T = 0.35$ and (c) $T = 0.7$ during heating.

In the snapshots in Fig. 9, the crystalline regions resemble the early stages of lamella formation. The shape of the crystalline region, particularly at the top surface, is similar to that observed in simulations of polyethylene crystallisation [22] and PVA in a confined system [8], where the width of the lamella structures correspond to stem lengths. We observe that, while chains belonging to lamella lie flat against the filler surface, the orientation of a given lamella appears to be random. We note that while corrugated or structured surfaces may give rise to specific crystal orientations, the smooth surface used here enables various orientations.

The effect of cooling rate on crystallisation temperature is shown in Fig. 10. For the highest cooling rate, $10\Gamma_0$ we can see that the stem mass fraction undergoes only a very small growth, and reaches only about 0.02 at $T = 0.35$. Conversely, the slowest cooling rates give the system time for crystal growth, and at $T = 0.35$ the stem mass fraction reaches around 0.40. We also see changes in the crystallisation temperature T_c, with T_c appearing to occur at higher temperature for slower growth rates, consistent with a previous simulation of PVA homogeneous crystallisation [13] and experimental observations. Recently the effect of cooling rate on nucleation in paraffins [23] was studied, albeit for a melt, where it was found that above a threshold cooling rate the system does not nucleate crystal structures.

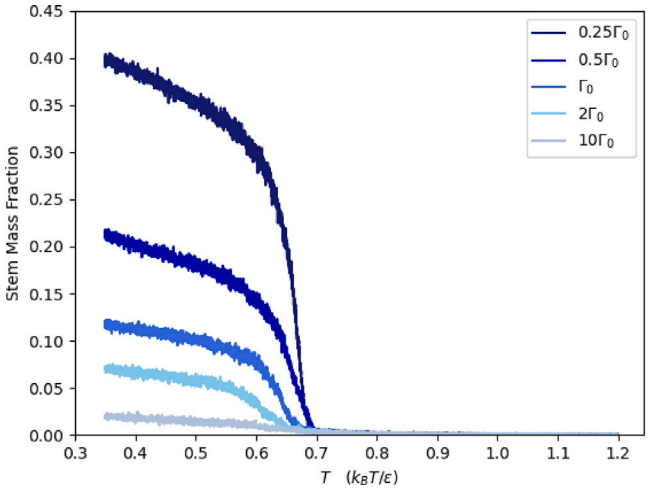

Fig. 10. Variation of stem mass fraction with cooling rate for the $\kappa_\theta = 2.4$ system with a wall interaction strength of $\epsilon_w = 1.80$.

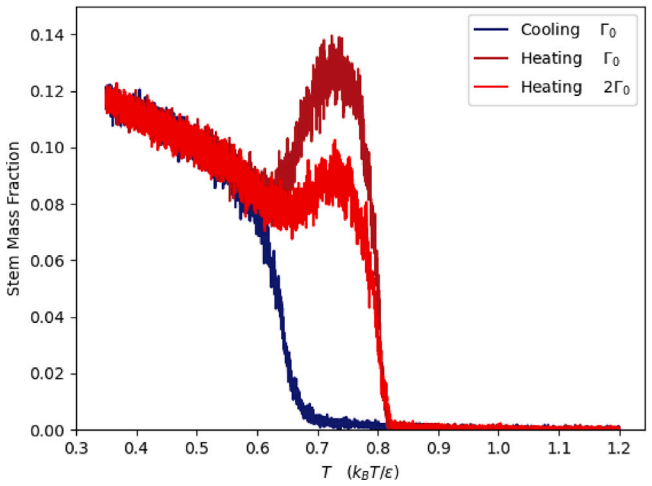

Fig. 11. Cooling and heating cycle for the $\kappa_\theta = 2.4$ system with a wall interaction strength of $\epsilon_w = 1.8$. The blue curve is cooling at a rate of Γ_0 from a melt state at $T = 1.2$ to $T = 0.35$. Starting from this state, the system is then heated from $T = 0.35$ to $T = 1.2$ at rates of Γ_0 and $2\Gamma_0$. (For interpretation of the references to colour in this figure legend, the reader is referred to the web version of this article.)

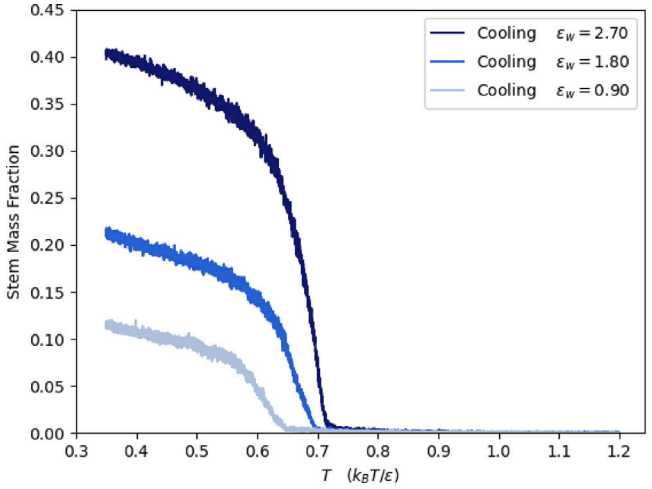

Fig. 12. Stem mass fraction vs temperature on cooling and then heating for different surface interaction strengths, ϵ_w, using a cooling rate of $0.5\Gamma_0$.

The effect of heating rate on melting temperature and hysteresis is shown in Fig. 11. The system is first cooled from a melt state at $T = 1.2$ to $T = 0.35$ at a cooling rate of Γ_0, as shown in Fig. 10, and this is then used as the starting point for two heating simulations from $T = 0.35$ to $T = 1.2$ at rates of Γ_0 and $2\Gamma_0$. The variation of stem mass fraction with temperature for these simulations is shown in Fig. 11. For both heating rates, we observe crystal growth between $T \approx 0.65$ to $T \approx 0.75$. Both heating rates show a strong hysteresis effect and melting occurs at approximately the same temperature. This crystal growth on heating is similar to experimentally observed cold crystallisation, where samples are observed to crystallise further on heating between T_g and T_m.

Now we investigate the effect of varying the wall interaction strength, ϵ_w. In Fig. 12, we show cooling curves for three different surface interaction strengths, $\epsilon_w = 0.9$, $\epsilon_w = 1.8$ used in the previous surface simulations, and $\epsilon_w = 2.7$. To allow for greater crystal growth, the systems were cooled from $T = 1.2$ to $T = 0.35$ at a rate of $0.5\Gamma_0$.

The weakest surface interaction strength of $\epsilon_w = 0.9$ shows an onset of crystallisation at $T_c \approx 0.65$ and reaches a stem mass fraction of about 0.12. Doubling the interaction strength to $\epsilon_w = 1.8$ has an earlier onset of crystallisation and almost doubles the final stem mass fraction to around 0.22. Further increasing the wall strength to $\epsilon_w = 2.7$ has an even earlier onset of crystallisation and increases the crystal fraction amount to around 0.41. The increase in crystallinity with increasing surface interaction strength is in agreement with a Monte Carlo study of isothermal crystallisation [24].

These findings are in agreement with those of Luo and Sommer [8] who found that heterogeneous nucleation occurred at a higher T_c than homogeneous nucleation. They attributed this acceleration in nucleation at the surface to an increase in entanglement length at the surface and crystallisation as a partial disentanglement process. However, we note that in our simulations the 20-bead chains are only comparable to the entanglement length and yet we also observe a higher T_c for the surface system. Instead, we rationalise our results in terms of the attractive wall potential lowering the free energy barrier to nucleation. Fig. 3 in the SI shows the stem mass fraction during cooling for 40-bead chains. The total stem mass fraction measured here is lower than that measured for 20-bead chains, although the temperature at which maximum growth is measured is the same for both chain systems. This supports our decision to study the 20-bead chains to understand the influence of a filler surface on nucleation.

We consider a schematic of the free energy vs temperature for melt and crystal systems in Fig. 13. First, we consider the bulk system in the absence of a surface, represented in Fig. 13a). At high temperatures, far above T_g and T_m, the polymer chains are in a melt state. As the temperature is lowered, the free energy of the melt increases and at T_m the melt and crystal free energies cross over. However, on cooling, the system will typically overshoot this cross over as there is a barrier to chain straightening and crystallisation. Instead, the system will continue to cool in the melt phase until it forms a small crystal nucleus. If the nucleus is larger than the critical nucleus size then the crystal will grow and the free energy of the system will drop towards that of the perfect crystal free energy, corresponding to the crystallisation temperature T_c. For a faster cooling rate the system does not have sufficient time to overcome the barriers and nucleation and growth will occur at a lower T_c. At very high cooling rates, the melt will not have sufficient time to crystallise at all, and at T_g will enter a glassy state, as we have seen in the simulations of the bulk polymer.

Now we consider the addition of a surface, which is known to facilitate heterogeneous nucleation. The attractive surface interaction lowers the free energy of the crystal nucleus at the surface so that nucleation and growth occurs at a higher T_c. In addition, the barrier to nucleation is lowered at the surface, due to the chain alignment as seen in Fig. 9. As the surface interaction increases, the free energy of the nucleus decreases, so that the crossover with the melt free energy occurs at higher T_c.

4. Conclusions

In this work we studied polymer heterogeneous nucleation using molecular dynamics simulations of a modified Kremer–Grest model. We first explored how chain stiffness influenced homogeneous nucleation and found that stiffer chains crystallised more readily than more flexible chains. For a system with stiff chains, it was observed that upon cooling the density, radius of gyration and stem mass fraction all sharply increased at temperature T_c, then continued to slowly increase upon further cooling. Upon subsequent heating the stem mass fraction initially decreased, following the cooling curve, until between T_g and T_c when it started to increase due to crystal growth, showing a strong deviation from the cooling curve, before melting at T_m. For the more flexible systems, a very small increase in stem mass fraction was observed, but the heating curve followed the cooling curve, and it was concluded that hysteresis could be used as a signature of crystallisation.

To investigate heterogeneous nucleation we selected a chain stiffness that did not readily exhibit homogeneous crystallisation. Cooling and heating cycles showed hysteresis, clearly demonstrating that the surface induced nucleation. Snapshots revealed that the crystal regions

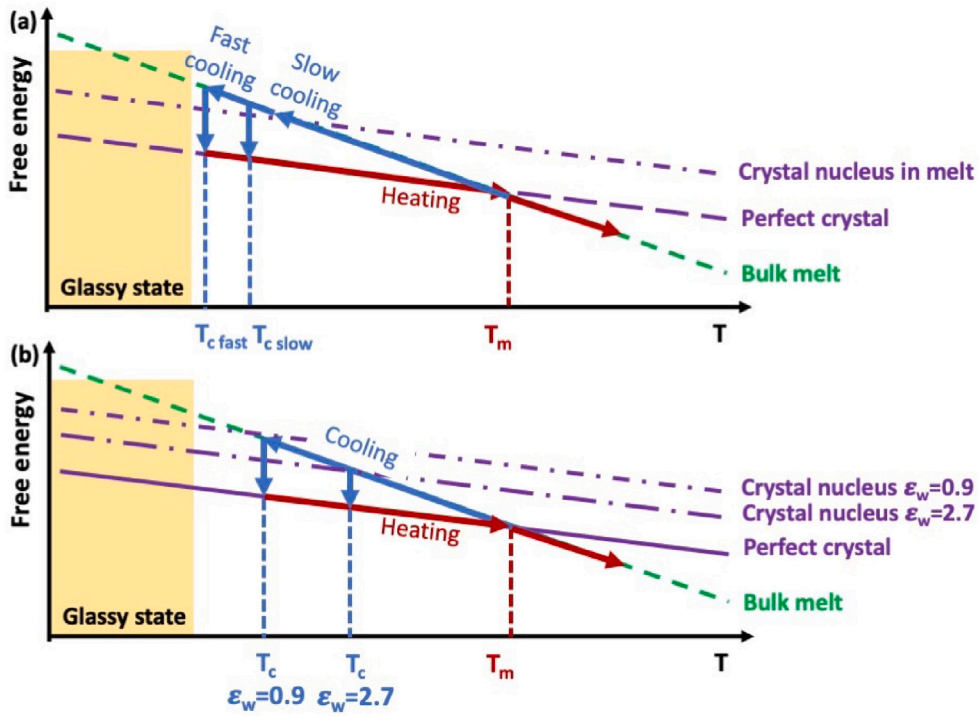

Fig. 13. Schematic of melt and crystal free energies as a function of temperature. (a) shows the behaviour of T_c with cooling rate, and (b) shows the behaviour of T_c with surface interaction strength ϵ_w. For chains with stiffness $\kappa_\theta = 2.4$ the glassy region begins at approximately T = 0.51, which marks the high temperature boundary of the glassy state.

occurred at the surfaces and resembled lamella-like structures. The cooling rate was varied and it was found that slower cooling rates resulted in a higher T_c and also in a significantly higher stem mass fraction, which is consistent with experimental observation. A slower heating rate gave an increased crystal growth rate below T_m. The polymer-surface interaction strength was varied, and it was found that increasing the interaction strength, resulted in an increase in T_c, and a significant increase in stem mass fraction.

In summary, we have shown that this polymer model system can capture essential polymer behaviour including homogenous and heterogeneous nucleation, enabling a deeper insight into how filler particles control polymer crystal nucleation. This will pave the way to the design of filler particles that can be tailored to tune plastic properties for use in specific applications.

CRediT authorship contribution statement

Dominic Wadkin-Snaith: Conceptualisation, Methodology, Software, Formal analysis, Investigation, Writing – original draft. **Paul Mulheran:** Writing – review & editing, Formal analysis, Supervision. **Karen Johnston:** Writing – review & editing, Formal analysis, Supervision, Project administration, Funding acquisition.

Declaration of competing interest

The authors declare that they have no known competing financial interests or personal relationships that could have appeared to influence the work reported in this paper.

Data availability

Input files will be made available as a dataset linked by a doi.

Acknowledgements

The authors would like to thank Katarzyna Majerczak, Vitor Magueijo and John Liggat for valuable discussions. The authors gratefully acknowledge funding from a UKRI Smart Sustainable Plastic Packaging, United Kingdom grant (NE/V010603/1). Results were obtained using the ARCHIE-WeSt High Performance Computer (www.archie-west.ac.uk) based at the University of Strathclyde.

Appendix A. Supplementary data

Supplementary material related to this article can be found online at https://doi.org/10.1016/j.polymer.2023.126113.

References

[1] Katarzyna Majerczak, Dominic Wadkin-Snaith, Vitor Magueijo, Paul Mulheran, John Liggat, Karen Johnston, Polyhydroxybutyrate: A review of experimental and simulation studies of the effect of fillers on crystallinity and mechanical properties, Polym. Int. 71 (2022) 1398–1408.
[2] N. Waheed, M.S. Lavine, G.C. Rutledge, Molecular simulation of crystal growth in n-eicosane, J. Chem. Phys. 116 (2002) 2301–2309.
[3] N. Waheed, M.J. Ko, G.C. Rutledge, Molecular simulation of crystal growth in long alkanes, Polymer 46 (20) (2005) 8689–8702.
[4] Takashi Yamamoto, Molecular dynamics modeling of polymer crystallization from the melt, Polymer 45 (4) (2004) 1357–1364.
[5] F. Varnik, J. Baschnagel, K. Binder, Reduction of the glass transition temperature in polymer films: A molecular-dynamics study, Phys. Rev. E (2002).
[6] Paul Z. Hanakata, Jack F. Douglas, Francis W. Starr, Local variation of fragility and glass transition temperature of ultra-thin supported polymer films, J. Chem. Phys. 137 (2012) 244901.
[7] Mark E. Mackura, David S. Simmons, Enhancing heterogenous crystallization resistance in a bead-spring polymer model by modifying bond length, J. Polym. Sci. Part B: Polym. Phys. 52 (2) (2014) 134–140.
[8] Chuanfu Luo, Martin Kröger, Jens-Uwe Sommer, Molecular dynamics simulations of polymer crystallization under confinement: Entanglement effect, Polymer 109 (2017) 71–84.
[9] Wolfgang Paul, Do Y. Yoon, Grant D. Smith, An optimized united atom model for simulations of polymethylene melts, J. Chem. Phys. 103 (4) (1995) 1702–1709.

[10] Kurt Kremer, Gary S. Grest, Dynamics of entangled linear polymer melts: A molecular-dynamics simulation, J. Chem. Phys. 92 (8) (1990) 5057–5086.
[11] Gary S. Grest, Kurt Kremer, Molecular dynamics simulation for polymers in the presence of a heat bath, Phys. Rev. A 33 (1986) 3628–3631.
[12] Hendrik Meyer, Florian Müller-Plathe, Formation of chain-folded structures in supercooled polymer melts, J. Chem. Phys. 115 (2001) 7807–7810.
[13] Hendrik Meyer, Florian Müller-Plathe, Formation of chain-folded structures in supercooled polymer melts examined by MD simulations, Macromolecules 35 (4) (2002) 1241–1252.
[14] Xiaoyan Qiu, Yongqiang Zhang, Haitao Wu, Rui Yang, Jun Yang, Rongjuan Liu, Yong Liu, Zhiping Zhou, Tongfan Hao, Yijing Nie, Blocked crystallization in capped ultrathin polymer films studied by molecular simulations, Polym. Int. 68 (2) (2019) 218–224.
[15] Christoph Bennemann, Wolfgang Paul, Kurt Binder, Burkhard Dünweg, Molecular-dynamics simulations of the thermal glass transition in polymer melts: α-relaxation behavior, Phys. Rev. E 57 (1998) 843–851.
[16] Aidan P. Thompson, H. Metin Aktulga, Richard Berger, Dan S. Bolintineanu, W. Michael Brown, Paul S. Crozier, Pieter J. in 't Veld, Axel Kohlmeyer, Stan G. Moore, Trung Dac Nguyen, Ray Shan, Mark J. Stevens, Julien Tranchida, Christian Trott, Steven J. Plimpton, LAMMPS - a flexible simulation tool for particle-based materials modeling at the atomic, meso, and continuum scales, Comput. Phys. Comm. 271 (2022) 108171.
[17] William Humphrey, Andrew Dalke, Klaus Schulten, VMD – visual molecular dynamics, J. Mol. Graph. 14 (1996) 33–38.
[18] Peng Yi, C. Rebecca Locker, Gregory C. Rutledge, Molecular dynamics simulation of homogeneous crystal nucleation in polyethylene, Macromolecules 46 (11) (2013) 4723–4733.
[19] Amit Shavit, Robert A. Riggleman, Influence of backbone rigidity on nanoscale confinement effects in model glass-forming polymers, Macromolecules 46 (12) (2013) 5044–5052.
[20] David McKechnie, Jordan Cree, Dominic Wadkin-Snaith, Karen Johnston, Glass transition temperature of a polymer thin film: Statistical and fitting uncertainties, Polymer 195 (2020) 122433.
[21] Chuanfu Luo, Jens-Uwe Sommer, Disentanglement of linear polymer chains toward unentangled crystals, ACS Macro Lett. 2 (1) (2013) 31–34, PMID: 35581821.
[22] Tuukka Verho, Antti Paajanen, Jukka Vaari, Anssi Laukkanen, Crystal growth in polyethylene by molecular dynamics: The crystal edge and lamellar thickness, Macromolecules 51 (13) (2018) 4865–4873, 30258252.
[23] Victor M. Nazarychev, Artyom D. Glova, Sergey V. Larin, Alexey V. Lyulin, Sergey V. Lyulin, Andrey A. Gurtovenko, Cooling-rate computer simulations for the description of crystallization of organic phase-change materials, Int. J. Mol. Sci. 23 (23) (2022).
[24] Tongfan Hao, Yongqiang Ming, Shuihua Zhang, Ding Xu, Rongjuan Liu, Zhiping Zhou, Yijing Nie, The influences of grafting density and polymer–nanoparticle interaction on crystallisation of polymer composites, Mol. Simul. 46 (9) (2020) 678–688.